High Energy Density and High Intensity Physics

Cellular irradiations with laser-driven carbon ions at ultra-high dose rates

Carbon is an ion species of significant radiobiological interest, particularly in view of its use in cancer radiotherapy, where its large Relative Biological Efficiency is often exploited to overcome radio resistance. A growing interest in highly pulsed carbon delivery has arisen in the context of the development of the FLASH radiotherapy approach, with recent studies carried out at dose rates of 40 Gy s^{-1}. Laser acceleration methods, producing ultrashort ion bursts, can now enable the delivery of Gy-level doses of carbon ions at ultra-high dose rates (UHDRs), exceeding 10^9 Gy s^{-1}. While studies at such extreme dose rate have been carried out so far using low LET particles such as electrons and protons, the radiobiology of high-LET, UHDR ions has not yet been explored. Here, we report the first application of laser-accelerated carbon ions generated by focussing 10^{20} Wcm^{-2} intense lasers on 10–25 nm carbon targets, to irradiate radioresistant patient-derived Glioblastoma stem like cells (GSCs).

Authors: S.J. McMahon, K.M. Prise, A. McIlvenny, A. McMurray, K. Polin, M. Borghesi, G. Milluzzo, H. Ahmed, C. Maiorino, L. Romagnani, D. Doria, S.W. Botchway, P.P. Rajeev

Contact authors: P. Chaudhary (p.chaudhary@qub.ac.uk)
M. Borghesi (m.borghesi@qub.ac.uk)
K.M. Prise (k.prise@qub.ac.uk)

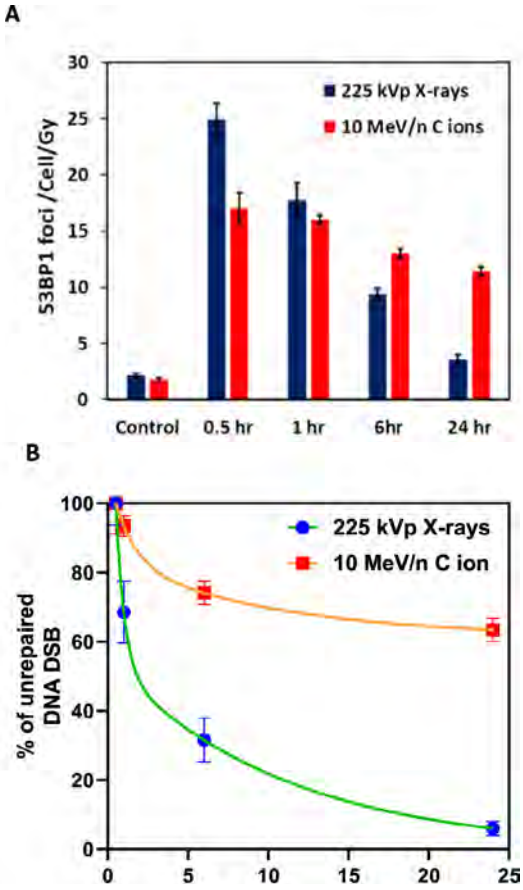

A). DNA DSB damage induced by 1 Gy of 225 kVp X-rays or 10 MeV n^{-1} laser-driven carbon ions and repair kinetics studied through 53BP1 foci formation assay. 53BP1 foci are expressed as mean no. of foci per cell per Gy. (B) DNA DSB repair expressed as percentage of unrepaired DNA DSB obtained by normalizing the amount of unrepaired DNA DSB at different time points, to the amount of unrepaired DNA DSB observed at 30 min (Error bars represent Standard deviation). The percentage repair kinetics over time is fitted with a two-phase decay analysis function (orange line carbon ions and green line x-rays) available in Graph pad Prizm software version 9.

Gas Target Characterization at OPAL

Plasma fluorescence measurements were performed for two different multi-centimetre laser wakefield targets. These measurements demonstrate the usefulness of this technique for target characterization. The gas cell target was shown to be uniform, while the gas jet target was shown to have a density dip of ~20%.

Authors: L. Feder, J. Chappell, J. Cowley, E. Archer, S. Kalos, D. McMahon, W. Wang, R. Walczak, S.M. Hooker

Contact author: L. Feder (linus.feder@physics.ox.ac.uk)

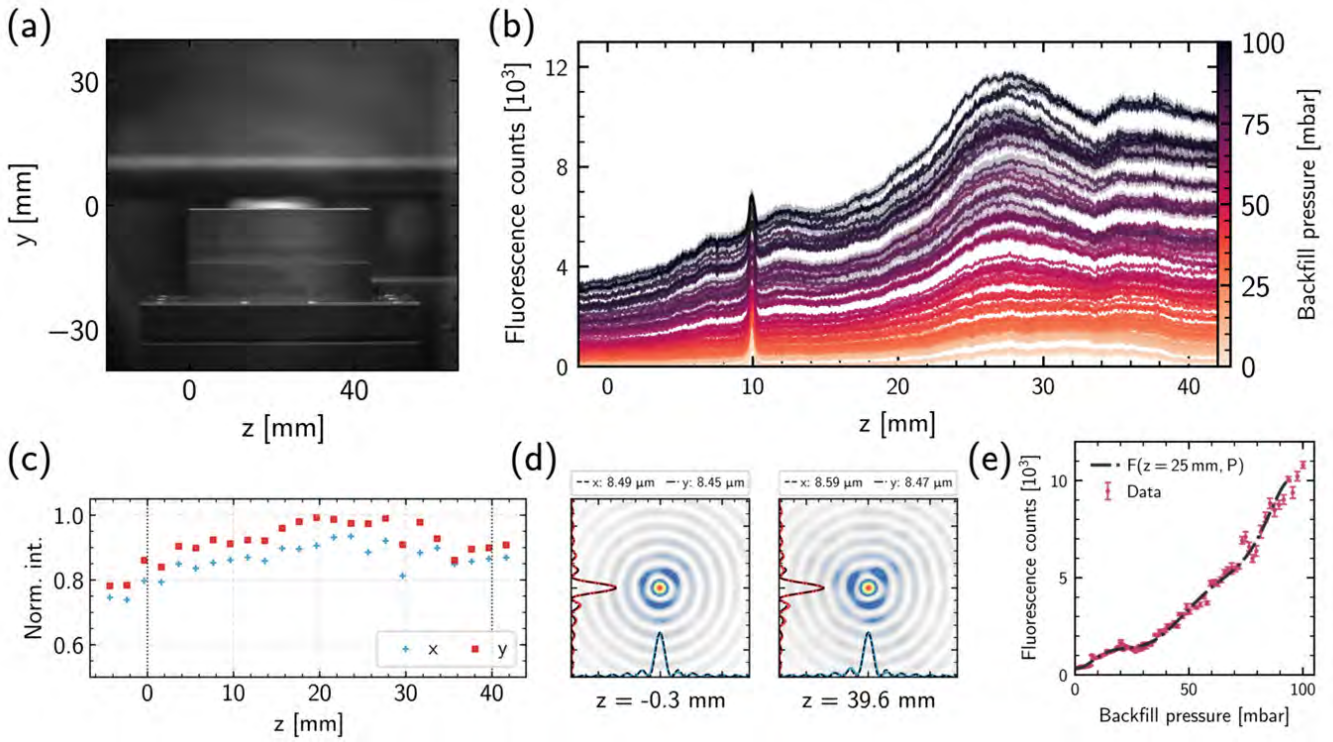

Figure 1: (a) Image of the 40 mm-long slit jet in place at OPAL; (b) example calibration curves demonstrating the measured average longitudinal fluorescence as a function of the backfill pressure; (c) measurements of the normalised peak intensity of the axicon focus at the position of the slit-jet; (d) measured axicon focal spots at either end of the slit-jet, with fits to the transverse intensity profiles; (e) example backfill calibration curve for z = 25 mm.

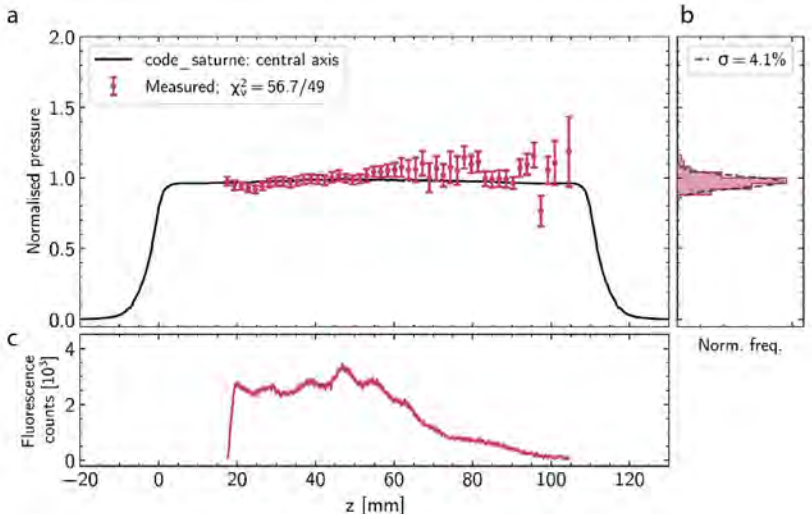

Figure 2: (a) Measurement of the pressure of the gas cell vs longitudinal position, along with the predicted profile from fluid simulations; (b) histogram of the measurements; (c) raw fluorescence signal from the cell.

Gas Target Design and Characterisation for EPAC EA1

Experimental Area 1 (EA1) in the Extreme Photonics Applications Centre (EPAC) will predominantly support experiments that utilise a long focal length parabola to focus the laser onto a gas target to generate high energy electrons and x-rays. The gas density profile can be tailored to favour the accelerator properties required for a particular application. The EPAC facility will provide users with a number of facility designed, characterised and maintained options for gas targetry depending on their requirements. The first design is a rectangular gas jet nozzle. Fluid simulations have been performed to design a prototype, which has been manufactured. Preliminary characterisation has been done on the manufactured nozzle by measurement of the nozzle throat size, and of the density profile through interferometry.

Authors: O.J. Finlay, N. Bourgeois, A. Stallwood, D.R. Symes, X.J. Gu, B. John, D.R. Emerson, L. Feder

Contact author: O. Finlay (oliver.finlay@stfc.ac.uk)

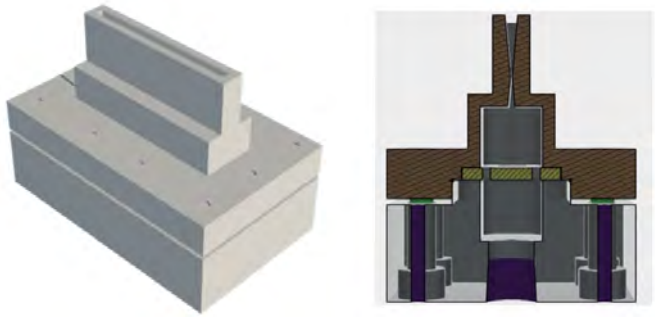

Figure 1: CAD drawing of the designed slot nozzle.

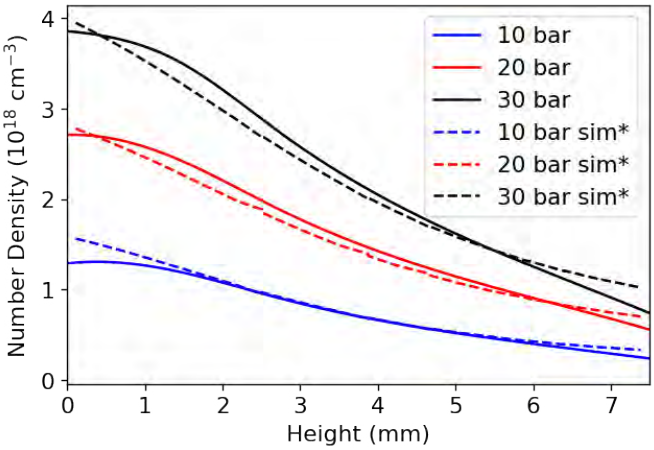

Figure 2: Neutral gas density measurement with probe traversing long direction of 40 mm EPAC slot nozzle. Simulation scaled to match inefficiency in gas line experimentally.

Automated control and optimization of laser-driven ion acceleration

The interaction of relativistically intense lasers with opaque targets represents a highly non-linear, multi-dimensional parameter space. This limits the utility of sequential 1D scanning of experimental parameters for the optimization of secondary radiation, although to-date this has been the accepted methodology due to low data acquisition rates. High repetition-rate (HRR) lasers augmented by machine learning present a valuable opportunity for efficient source optimization. Here, an automated, HRR-compatible system produced high-fidelity parameter scans, revealing the influence of laser intensity on target pre-heating and proton generation. A closed-loop Bayesian optimization of maximum proton energy, through control of the laser wavefront and target position, produced proton beams with equivalent maximum energy to manually optimized laser pulses but using only 60% of the laser energy. This demonstration of automated optimization of laser-driven proton beams is a crucial step towards deeper physical insight and the construction of future radiation sources.

Authors: B. Loughran, M.J.V. Streeter, M. Borghesi, C. Hyland, P. Parsons, O. McCusker, C.A.J. Palmer, H. Ahmed, S. Astbury, N. Bourgeois, S.J.D. Dann, T. Dzelzainis, J.S. Green, C. Spindloe, D.R. Symes, M. Balcazar, S. Dilorio, A.G.R. Thomas, C.B. Curry, N.P. Dover, O.C. Ettlinger, G.S. Hicks, Z. Najmudin, N. Xu, M. Gauthier, S.H. Glenzer, L. Giuffrida, G.D. Glenn, R.J. Gray, M. King, P. McKenna, V. Istokskaia, D. Margarone, C. Parisuaña, F. Treffert

Contact author: B. Loughran (bloughran08@qub.ac.uk)

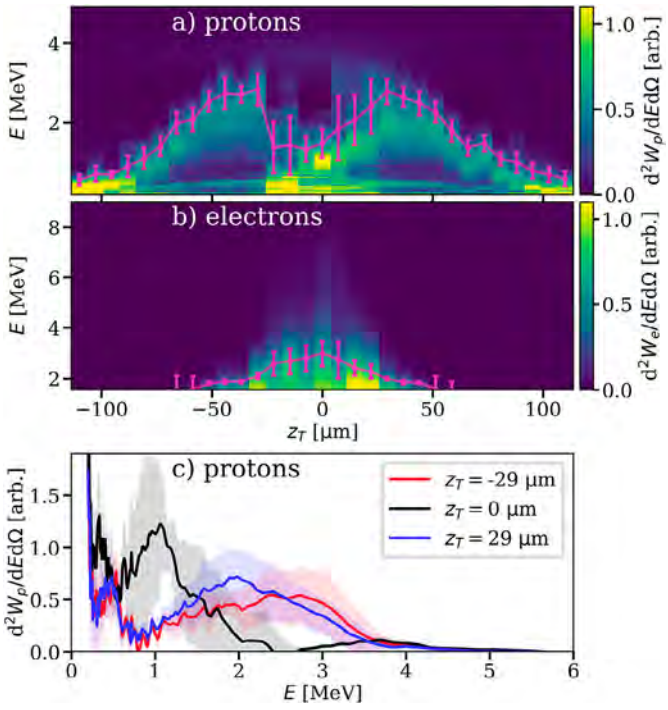

a) Proton and (b) electron energy spectra from the rear side of the target during an automated target position scan (z_T) with a 12 μm Kapton tape and an on-target laser energy of 438±32 mJ. (c) Average proton spectra (and standard deviation) for different z_T positions as indicated in the legend. The proton spectra are recorded by the time-of-flight diamond detector. Each column of the waterfall plots is the average of the 10 shots from each burst. The scan comprises 31 bursts at different target positions spaced at 7.3 μm intervals along the laser propagation axis. Negative values of z_T are when the target plane is closer to the incoming laser pulse and z_T = 0 is the target at the best focus of the laser pulse. The magenta data points, connected with a guideline, indicate the burst-averaged 95th percentile energy as well as the standard deviation of this value across the burst.

Development of a laser driven electron source for radiobiological applications

We report on the characterisation of a laser driven electron source for radiobiological applications. Doses in excess of 3 Gy were generated by a laser driven plasma wakefield accelerator. The electron beam duration is expected to have a duration on the order of 20 fs indicating unprecedented dose-rates in excess of 10^{13} Gy/s are expected. The stability of the source was characterised and its applications to radiobiological research discussed.

Authors: C.A. McAnespie, M.J.V. Streeter, L. Calvin, N. Cavanagh, K. Fleck, G. Sarri, P. Chaudhary, S.J. McMahon, K.M. Prise, B. Kettle, S.W. Botchway, S. Needham, N. Bourgeois

Contact author: C.A. McAnespie (cmcanespie01@qub.ac.uk)

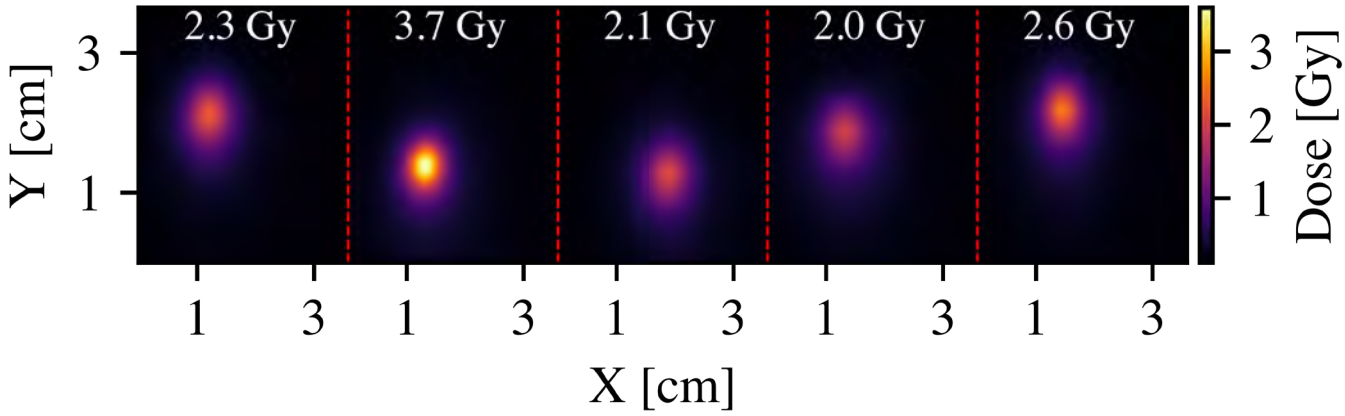

Dose profile and pointing stability for 5 consecutive shots after optimisation. The peak dose for each shot is printed in white. Consecutive shots are separated by a dashed red line.

Characterisation of an all-optical inverse Compton scattering source for industrial imaging

We report on the production of an all-optical inverse Compton scattering (ICS) source for industrial imaging, generated using a two-laser configuration. Successful laser-electron ICS interactions were obtained for electron energies up to ~1 GeV, with numerical estimates suggesting photon energies in the range of approximately 1 - 10 MeV were achieved. The duration of the photon bunch can be estimated as 50 fs, with a source size on the order of 10 μm. Imaging of reference line pairs was used to demonstrate a resolution of 170 μm, highlighting the unique advantages of this source. A copper test object was used to demonstrate the capability for high energy tomographic scanning.

Authors: C.A. McAnespie, M.J.V. Streeter, L. Calvin, N. Cavanagh, K. Fleck, G. Sarri, B. Kettle, O. Finlay, K. Fedorov, C.D. Armstrong, S.J.D. Dann, B. Spiers, D.R. Symes, W. Sun, J.M. Warnett, E. Kiely

Contact author: C.A. McAnespie (cmcanespie01@qub.ac.uk)

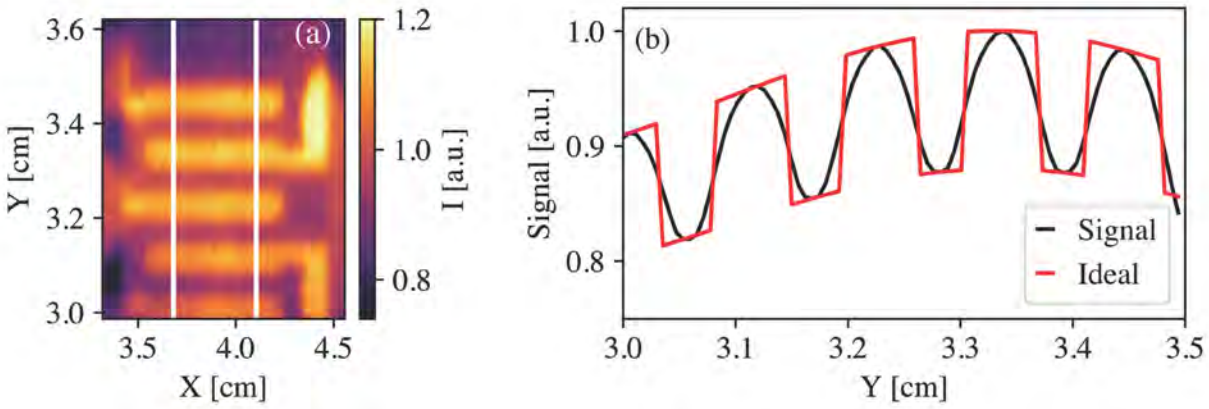

Figure 1: (a): Single shot projection of the resolution grid taken with a magnification of 1.75. The dark and light features highlighted between the two white lines are 400 μm line pairs. (b) The signal (black) averaged between the white banded region of (a). An ideal projection with infinite resolution and zero source size is given in red.

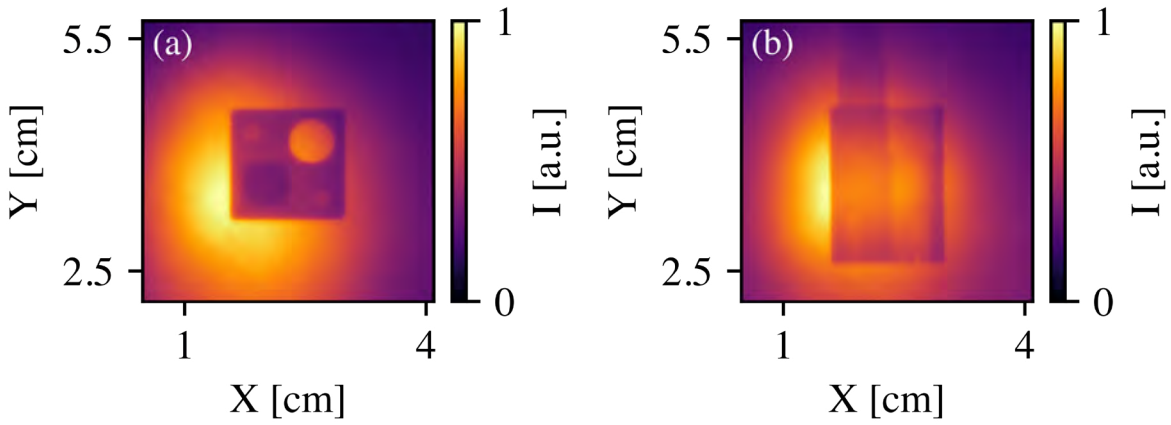

Figure 2: (a) Raw projection at 0 degrees; (b) raw projection at 90 degrees. A filter has been used to remove hot pixels from hard x-ray hits.

Versatile tape-drive for high-repetition-rate laser-driven proton acceleration

We present the development and characterization of a high-stability, multi-material, multi-thickness tape-drive target for laser-driven acceleration at repetition rates of up to 100 Hz. The tape surface position was measured to be stable on the sub-micrometre scale, compatible with the high-numerical aperture focusing geometries required to achieve relativistic intensity interactions with the pulse energy available in current multi-Hz and near-future higher repetition-rate lasers (> kHz). Long-term drift was characterized at 100 Hz demonstrating suitability for operation over extended periods. The target was continuously operated at up to 5 Hz in a recent experiment for 70,000 shots without intervention by the experimental team, with the exception of tape replacement, producing the largest data-set of relativistically intense laser-solid foil measurements to date. This tape drive provides robust targetry for the generation and study of high-repetition-rate ion beams using next-generation high-power laser systems, also enabling wider applications of laser-driven proton sources.

Reproduced from Xu N, Streeter MJV, Ettlinger OC, et al. High Power Laser Sci. Eng. ***11****, e23 (2023), under the terms of the Creative Commons Attribution 4.0 licence doi: 10.1017/hpl.2023.27*

Authors: N. Xu, O.C. Ettlinger, N.P. Dover, G.S. Hicks, Z. Najmudin, M.J.V. Streeter, M. Borghesi, C. Hyland, B. Loughran, O. McCusker, P. Parsons, C.A.J. Palmer, H. Ahmed, S. Astbury, N. Bourgeois, S.J.D. Dann, T. Dzelzainis, J.S. Green, C. Spindloe, D.R. Symes, C.B. Curry, V. Istokskaia, M. Gauthier, S.H. Glenzer, L. Giuffrida, G.D. Glenn, R.J. Gray, M. King, P. McKenna, D. Margarone, C. Parisuaña, F. Treffert

Contact author: C.A.J. Palmer (c.palmer@qub.ac.uk)

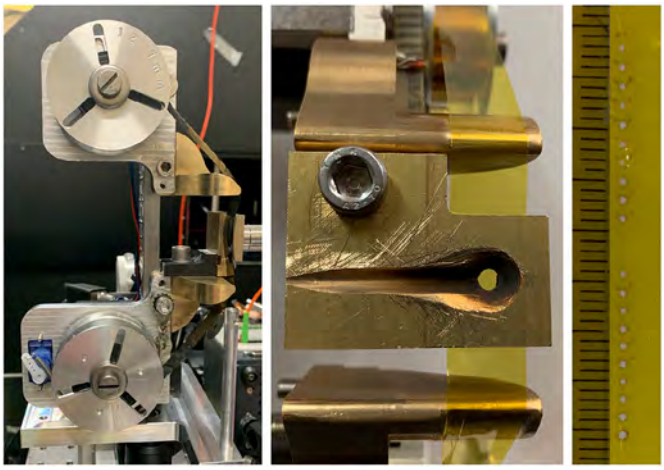

Figure 1: (left) Photograph showing the spools of the drive and the brass frame supporting the tape; (centre) photograph showing tape running vertically on the brass supports. The interaction point is at the centre of the hole, with a groove cut away to provide diagnostic access; (right) photograph of the tape after a series of shots with 400 mJ laser energy. The hole diameters are less than 1 mm diameter and spaced by approximately 2 mm when operating at a linear speed of 2 mm/s. The hardware is capable of speeds exceeding 500 mm/s.

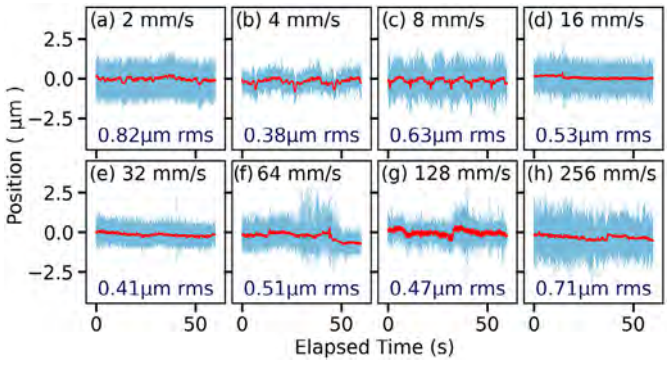

Figure 2: Tape positional jitter across a range of speeds over 1 minute operation. Low frequency movement (< 1 Hz), better representing the tape motion, is shown with the red line and the RMS variation in position is quoted in each subplot. In (c), the oscillations correspond to a resonance of the tape-drive structure. Faster speeds (> 8 mm/s) typically result in lower jitter amplitude because of reduced stepper motor vibration.

Characterization of laser wakefield acceleration efficiency with octave spanning near-IR spectrum measurements

We report on experimental measurements of energy transfer efficiencies in a GeV-class laser wakefield accelerator. Both the transfer of energy from the laser to the plasma wakefield and from the plasma to the accelerated electron beam was diagnosed by simultaneous measurement of the deceleration of laser photons and the acceleration of electrons as a function of plasma length. The extraction efficiency, which we define as the ratio of the energy gained by the electron beam to the energy lost by the self-guided laser mode, was maximized at 19 ± 3% by tuning the plasma density and length. The additional information provided by the octave-spanning laser spectrum measurement allows for independent optimization of the plasma efficiency terms, which is required for the key goal of improving the overall efficiency of laser wakefield accelerators.

*Reproduced from MJV Streeter et al. Phys. Rev. Accel. Beams **25**, 101302 (2022), published by the American Physical Society under the terms of the Creative Commons Attribution 4.0 licence doi: 10.1103/PhysRevAccelBeams.25.101302*

Authors: M.J.V. Streeter, Y. Ma, A.G.R. Thomas, B. Kettle, E. Gerstmayr, J.M. Cole, S.P.D. Mangles, Z. Najmudin, S.J.D. Dann, F. Albert, N. Lemos, N. Bourgeois, P.P. Rajeev, D.R. Symes, S. Cipiccia, I. Gallardo González, O. Lundh, A.E. Hussein, D.A. Jaroszynski, R. Spesyvtsev, G. Vieux , M. Shahzad, K. Falk, K. Krushelnick, R. Sandberg, N.C. Lopes, C. Lumsdon, M. Smid

Contact authors: M.J.V. Streeter (m.streeter@qub.ac.uk)

A.G.R. Thomas (agrt@umich.edu)

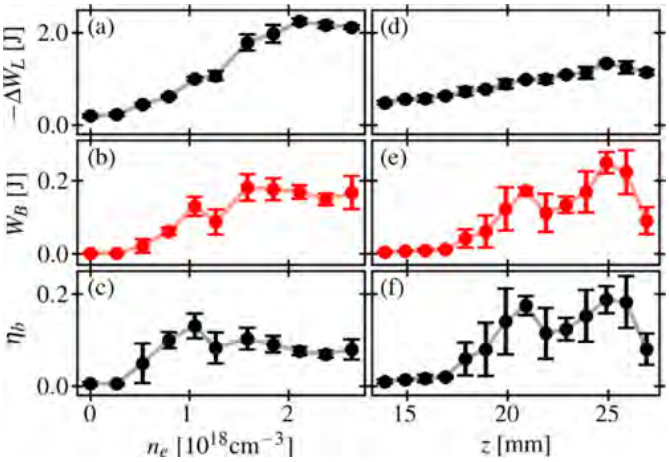

Figure 1: Laser energy loss, electron beam energy, and extraction efficiency as functions of plasma density for z = 27 mm (a)–(c), and length (d)–(f) with n_e = 1.25 x 10^{18} cm^{-3}.

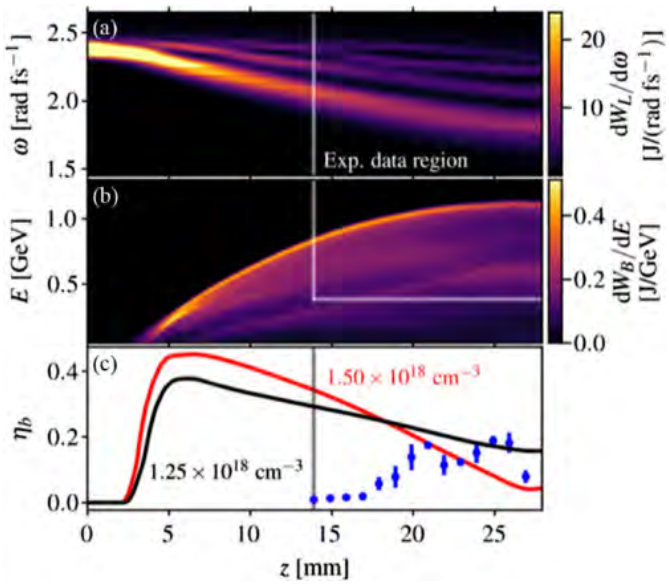

Figure 2: (a) Laser and (b) electron spectra as functions of propagation distance taken from a PIC simulation with a plateau density of n_e = 1.25 x 10^{18} cm^{-3}. (c) The extraction efficiency, calculated as the ratio of the electron beam energy to the laser energy loss, for simulations with n_e = (1.25, 1.5) x 10^{18} cm^{-3} and the experimental measurements (blue points) at n_e = 1.25 x 10^{18} cm^{-3}.

Laser wakefield accelerator modelling with variational neural networks

A machine learning model was created to predict the electron spectrum generated by a GeV-class laser wakefield accelerator. The model was constructed from variational convolutional neural networks, which mapped the results of secondary laser and plasma diagnostics to the generated electron spectrum. An ensemble of trained networks was used to predict the electron spectrum and to provide an estimation of the uncertainty of that prediction. It is anticipated that this approach will be useful for inferring the electron spectrum prior to undergoing any process that can alter or destroy the beam. In addition, the model provides insight into the scaling of electron beam properties due to stochastic fluctuations in the laser energy and plasma electron density.

Reproduced from M.J.V. Streeter et al., High Power Laser Science and Engineering, vol. 11, p. e9, 2023, published by the Cambridge University Press under the terms of the Creative Commons Attribution 4.0 licence doi: 10.1017/hpl.2022.47

Authors: M.J.V. Streeter, L. Calvin, N. Cavanagh, G. Sarri, C. Colgan, E.E. Los, R. Watt, E. Gerstmayr, B. Kettle, Z. Najmudin, S.P.D. Mangles, C.C. Cobo, C. Arran, C.D. Murphy, C.P. Ridgers, N. Bourgeois, S.J.D. Dann, P. Parsons, P.P. Rajeev, D.R. Symes, J. Carderelli, R. Fitzgarrald, Q. Qian, A.G.R. Thomas, A.S. Joglekar, P. Mckenna

Contact author: M.J.V. Streeter (m.streeter@qub.ac.uk)

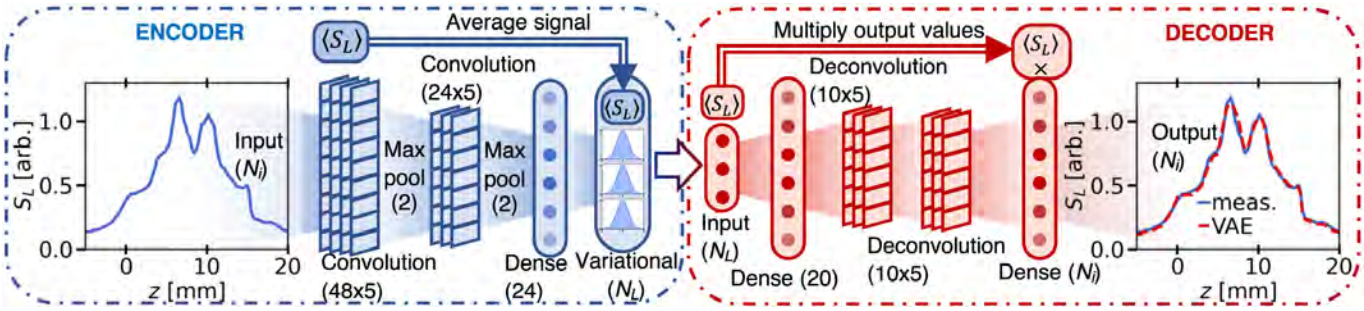

Variational autoencoder (VAE) architecture for determining the latent space representation of the diagnostics. The type and dimension of each layer are indicated in the labels. The inset plots show an example laser scattering signal S_L and the approximation returned by the VAE. The input (and output) size N_i is equal to the data binning of the results for each individual diagnostic. Max pooling was used at the output of each convolution layer, which combined neighbouring output pairs and returned only the maximum of each pair. The average signal, in this case $\langle S_L \rangle$ was passed as an additional latent space parameter for the encoder and was used to scale the output of the decoder. The autoencoder structure was the same for each diagnostic, except for the size of the latent space.

The role of transient plasma photonics structures in plasma-based amplifiers

High power lasers have become useful scientific tools, but their large size is determined by their low damage-threshold optical media. A more robust and compact medium for amplifying and manipulating intense laser pulses is plasma. Here we demonstrate, experimentally and through simulations, that few-millijoule, ultra-short seed pulses interacting with 3.5 J counter-propagating pump pulses in plasma, stimulate back-scattering of nearly 100 mJ pump energy with high intrinsic efficiency, when detuned from Raman resonance. This is due to scattering off a plasma Bragg grating formed by ballistically evolving ions. Electrons are bunched by the ponderomotive force of the beat-wave, which produces space-charge fields that impart phase correlated momenta to ions. They inertially evolve into a volume Bragg grating that backscatters a segment of the pump pulse. This ultra-compact, two-step, inertial bunching mechanism can be used to manipulate and compress intense laser pulses. We also observe stimulated Compton (kinetic) and Raman backscattering.

Reproduced from Vieux, G., Cipiccia, S., Welsh, G.H. et al. The role of transient plasma photonic structures in plasma-based amplifiers. Commun Phys ***6****, 9 (2023) under the terms of the Creative Commons Attribution 4.0 licence doi: 10.1038/s42005-022-01109-5*

Authors: G. Vieux, B. Ersfeld, E. Brunetti, S. Cipiccia, B. Eliasson, C. Picken, G. McKendrick, M.P. Tooley, G.H. Welsh, S.R. Yoffe, D.A. Jaroszynski, F. Gärtner, M-S. Hur, J.M. Dias, T. Kühl, G. Lehmann

Contact authors: G. Vieux (g.vieux@strath.ac.uk)

D.A. Jaroszynski (d.a.jaroszynski@strath.ac.uk)

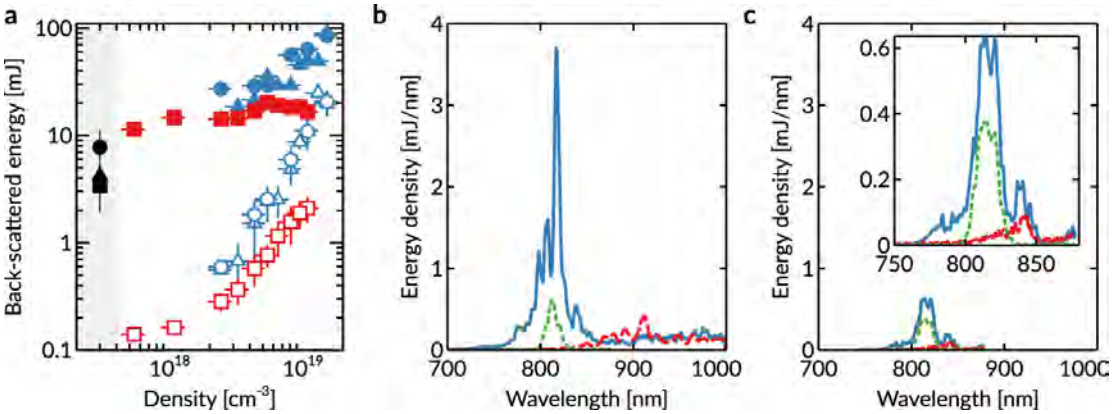

Main experimental results: **a** Back-scattered energy in the seed direction. Combined pump and seed shots are depicted by solid symbols, circle and triangle for positive frequency chirp, and square for negative frequency chirp. Empty symbols represent corresponding shots without the seed pulse i.e. scattering from noise. The different symbol shapes characterise different runs. The energy values are averages of three shots, with the error given as the standard deviation. Error on the inferred plasma density is estimated to be ±20%. Where the error bars are not visible, their lengths are smaller or equal to the symbol sizes. **b**, **c** are single-shot spectra. Solid (blue) line: seed spectrum after interaction; dotted (green) line: initial seed spectrum; dashed (red) line: spectrum of pump back-scattered signal without seed. Areas under the curves have been normalised to the measured energy, assuming that little energy falls outside the spectral window. **b** Pump with a positive frequency chirp, plasma density ~1.5×10^{19} cm^{-3} ($n_p/n_c \approx 8.6 \times 10^{-3}$); **c** Pump with a negative frequency chirp, plasma density ~10^{19} cm^{-3} ($n_p/n_c \approx 5.7 \times 10^{-3}$). The longest observable wavelength is ~880 nm because a different spectrometer grating was used compared to that in **b**. The inset in **c** displays the same data as **c** plotted on a magnified scale.

Laboratory study of the Biermann battery magnetic field compression in laser-produced plasma

In this work we present experimental results related to the collision of parallel magnetic fields and study the compression that ensues between them. For this, we use two dense, spatially separated, targets that are both irradiated by nanosecond laser beams. The generated magnetic fields, due to the Biermann battery effect close to the target surfaces, are clockwise with respect to the plasma expansion axis. The ablating plasmas radially expand and advect the aligned parallel magnetic fields to the interaction region between the targets. By shifting the targets along their normal, we enable these laterally expanding Biermann fields to collide, leading to magnetic field compression and accumulation in the gap between the targets. To resolve in time the topology of the compressed magnetic field we employ the proton deflectometry technique to diagnose each magnetic field and the magnetic field pile-up between the targets.

Authors: W. Yao, R. Lelièvre, J. Fuchs, H. Ahmed, D.C. Carroll, P. Antici, J. Béard, M. Borghesi, C. Fegan, P. Martin, A.F.A. Bott, S.N. Chen, A. Ciardi, E.D. Filippov, E. d'Humières, A. Sladkov, S. Pikuz

Contact author: J. Fuchs (julien.fuchs@polytechnique.edu)

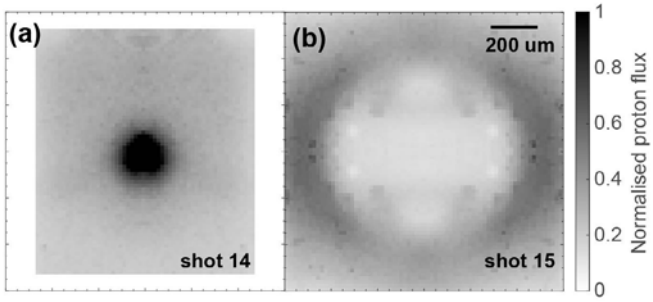

Figure 1: **Proton radiography results:** Experimental RCF measurements probing the single magnetic flux tubes produced on (a) target T2 or (b) target T1. Both images are snapshots taken at 1 ns.

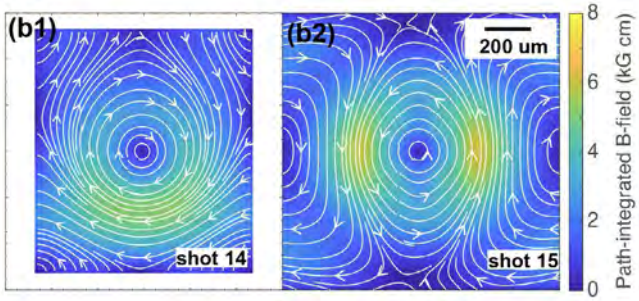

Figure 2: **Analysis of the RCF results:** Path-integrated magnetic field strength analysed via the code PROBLEM.[1] The white-arrow streamlines represent the in-plane magnetic field lines (Bx and By), and the colour-map shows the path-integrated (along the z-axis) strength of the xy-plane magnetic field.

[1] *Bott, A.F.A. et al. (2017) 'Proton imaging of stochastic magnetic fields', Journal of Plasma Physics, 83(6), p. 905830614. doi:10.1017/S0022377817000939*

High dose delivery in radiobiology experiments employing laser-driven protons

High energy protons accelerated by the Vulcan laser have been used, in several campaigns, to irradiate cells and investigate the biological effects of irradiations at ultra-high dose rates.

The use of a novel helical coil target design has enabled the production of highly collimated proton bunches, greatly increasing the dose delivered to the cells in the relevant energy ranges.

We discuss here the irradiation of cell samples using both the standard flat foil and helical coil target configurations, with the latter delivering very high doses to the cells of up to 70 Gy in a single irradiation. This large dose range enables clinically relevant studies of the effects of ultra-high dose rate on various cell types, in studies of potential relevance to the FLASH mechanism of radiotherapy and future approaches to cancer treatment.

Authors: P. Martin, O. Cavanagh, P. Chaudhary, C. Fegan, A. McCay, J. Morrow, S. Kar, M. Borghesi, K. Prise, H. Ahmed

Contact author: M. Borghesi (m.borghesi@qub.ac.uk)

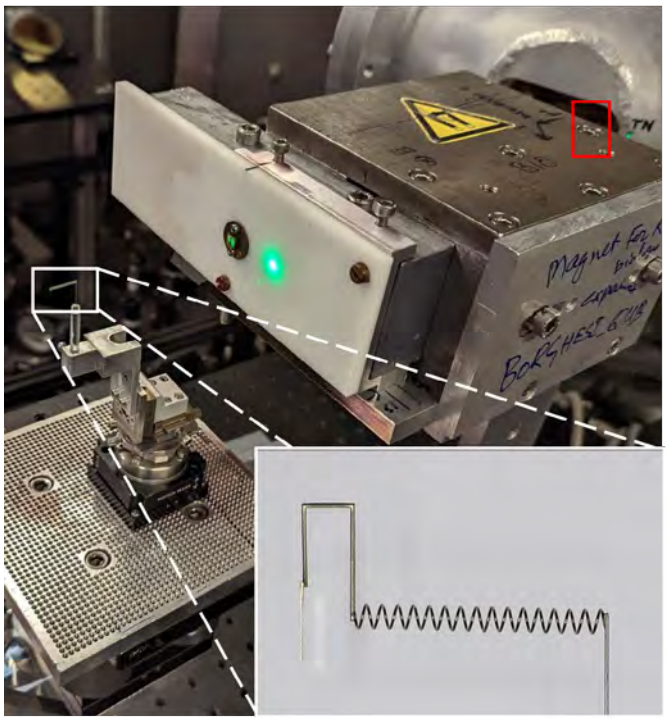

Figure 1: An image of the experimental setup for cell irradiation. A pinhole 8 cm from the target (indicated by the white box) leads into a dipole magnet, separating protons by their energy and leading to a Kapton window, behind which the cells are placed. The red box highlights the cell plane upon which 35 MeV protons were incident. Inset: Side view of a typical helical coil (HC) target used in the campaign, designed to produce a high flux of protons at around 35 MeV.

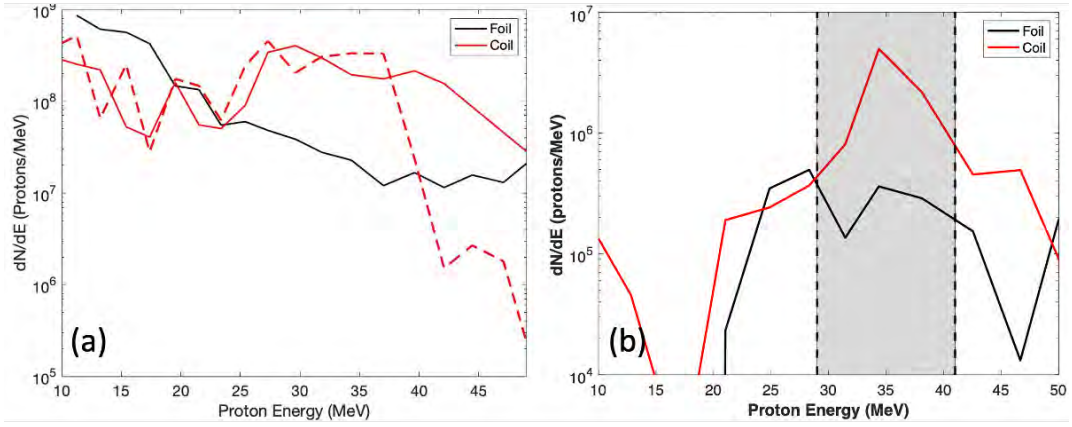

Figure 2: The proton spectrum from radiochromic film (RCF) for flat foils (black) and HC (red), with the RCF stack placed (a) before the magnet (~8 cm from the interaction point), and (b) after the magnet, at the cell plane. The dashed red line is a second HC shot, to demonstrate consistent flux around the 35 MeV point. The grey area indicates the approximate energy range by which the cells were irradiated.